International Journal of Biological Macromolecules 271 (2024) 132603

Contents lists available at ScienceDirect

International Journal of Biological Macromolecules

journal homepage: www.elsevier.com/locate/ijbiomac

The impact of surface functionalization of cellulose following simulated digestion and gastrointestinal cell-based model exposure

Amanda K. Charlton-Sevcik [a], Clancy Collom [a], James Y. Liu [a], You-Lo Hsieh [c], Nicole Stark [d], James D. Ede [b], Jo Anne Shatkin [b], Christie M. Sayes [a,*]

[a] Department of Environmental Science, Baylor University, One Bear Place #97266, Waco, TX 76798-7266, USA
[b] Vireo Advisors, LLC, Boston, MA 02130-4323, USA
[c] University of California – Davis, USA
[d] U.S. Forest Products Laboratory, USA

ARTICLE INFO

Keywords:
Nanocellulose
Read across
Gastrointestinal model
In vitro toxicology
Physicochemical characterization
Simulated digestion

ABSTRACT

Surface-functionalized cellulose materials are developed for various purposes, including food additives and food contact materials. A new biologically relevant testing strategy has been developed based on guidance from the European Food Safety Authority to demonstrate the safety of several next-generation surface-functionalized cellulose materials. This strategy involves a complex three-stage simulated digestion to compare the health effects of thirteen novel different types of cellulose. The physical and chemical properties of surface-functionalized fibrillated celluloses differed depending on the type, amount, and location of functional groups such as sulfonate, TEMPO-oxidized carboxy, and periodate-chlorite oxidized dicarboxylic acid celluloses. Despite exposure to gastrointestinal fluids, the celluloses maintained their physicochemical properties, such as negative surface charges and high length-to-width/thickness aspect ratios. An established intestinal co-culture model was used to measure cytotoxicity, barrier integrity, oxidative stress, and pro-inflammatory response to create a toxicological profile for these unique materials. We conclude that the C6 carboxylated cellulose nanofibrils by TEMPO-oxidation induced the most toxicity in the biological model used in this study and that the observed effects were most prominent at the 4-hour post-exposure time point.

1. Introduction

Cellulose nanomaterials (CNs), also called 'nanocelluloses', are cellulose nanocrystals (CNC) and cellulose nanofibrils (CNF) with rod and fibril diameter/width <100 nm. Related materials in this class of cellulose-based materials include microfibrillated (MFC) and microcrystalline celluloses (MCC), which have external dimensions in the micrometer size scale. The abundant hydroxyl groups on the CNs' surface give them inherent hydrophilicity and aqueous processibility. Still, they are incompatible and challenging to process with hydrophobic materials, such as composite materials, laminates, barrier films, and coatings being developed for food packaging. Such challenges have driven the development of novel functionalization of CNs *via* the reaction of their surface hydroxyls for improved compatibility with the organic polymers used in various commercial applications [1–3]. Over the past five years, the scientific community has focused on unmodified forms of CNF and CNC along with MFC to demonstrate their safety in manufacturing and food and consumer products [4–6]. However, little is known about functionalized CNs' environmental or human health effects.

Surface-functionalized CNs have already been used in some commercial products, with many more in development. One process attaches lignin to CNC and CNF surfaces, increasing the CNs' hydrophobicity and compatibility with plastics and polymers [7]. These CNs are combined with plastic or rubber to make lightweight automotive parts using the "Kyoto Process," which involves acetylating wood pulp before fibrillation [8]. Another process functionalized TEMPO-CNF (a method to oxidize cellulose using 2,2,6,6-tetramethylpiperidine-1-oxyl radical) with metal nanoparticles for antimicrobial and deodorizing composites in absorbent diapers and sanitary napkins [9]. TEMPO-CNF is also used to manufacture oxygen barrier films, superabsorbent materials, and lightweight composites for automotive industries [10–12]. There are over 150 known ways to modify the surface of CNs, and researchers are working to develop sustainable methods and safer products [13–15].

* Corresponding author at: Baylor University, Baylor Sciences Building, BSB Room B407, One Bear Place #97266, Waco, TX 76798-7266, USA.
E-mail address: Christie_sayes@baylor.edu (C.M. Sayes).

https://doi.org/10.1016/j.ijbiomac.2024.132603
Received 16 January 2024; Received in revised form 16 May 2024; Accepted 21 May 2024
Available online 22 May 2024

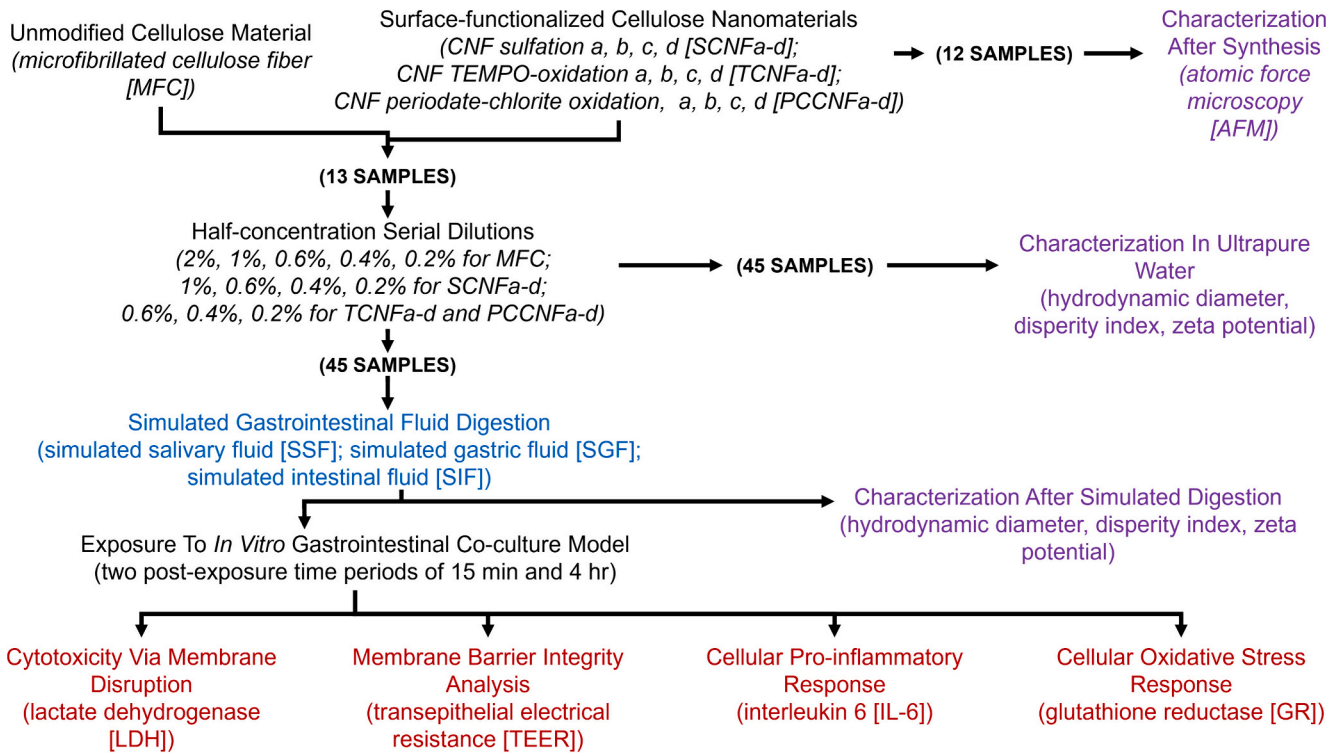

Fig. 1. Experimental design as described by the flow of samples throughout the study. One reference material (MFC) and twelve surface-functionalized cellulose nanomaterials (Table 1) were cataloged, dispersed in ultrapure water in equivalent concentrations (maximum of 1 % (wt/v)), and labeled. All CN samples were digested in salivary, gastric, and intestinal fluids and characterized for hydrodynamic size, dispersity index, and zeta potential (Table 2). Image analyses were performed *via* atomic force microscopy (Fig. 3). Lastly, the digested CN samples were exposed to an *in vitro* intestinal co-culture model (Fig. 2) and assessed for induced biological activity (Figs. 4–10).

Humans are exposed to cellulose through dermal, inhalation, and ingestion routes [16–19]. For example, occupational workers may be exposed to aerosolized cellulose fibers while producing food packaging materials containing cellulose. While handling the final products, workers and consumers may also come into dermal contact with cellulose. During the storage or heating of food package materials, cellulose could migrate from the packaging into food and subsequently be ingested. Therefore, when novel surface-functionalized CNs are used in products, it is necessary to assess the safety of these materials and identify the potential risks. Researchers conducting toxicological assessments have found that the surface characteristics of engineered nanomaterials play a critical role in influencing environmental and human health effects [20–24].

Product safety can be evaluated through animal (*in vivo*) and cell (*in vitro*) based testing models [25–29]. While animal studies may be necessary in some cases, they are time and resource-intensive, leading to a growing demand for alternative ways to test the safety of new substances. The U.S. Environmental Protection Agency and other organizations such as ECHA, EFSA, and Health Canada are dedicated to reducing and replacing animal testing with alternative strategies to promote safety. *In vitro* assessments have proven effective in demonstrating safety [30–33]. Through relevant testing, researchers can identify safer materials or manufacturing methods that are less likely to face regulatory hurdles and that can be adopted more quickly by the market [34–36].

This study aimed to identify the potential hazards of novel and conventional surface-functionalized cellulose-based materials [37–39]. The two-step approach used to achieve this goal was (1) to identify the most prominent surface functionalization for CNF with well-defined chemical and physical attributes proposed for use in composites and (2) to evaluate the safety of the twelve most representative surface-functionalized CNs for use in commercial products in the context of intentional or accidental ingestion. These results provide safety data to advance regulatory acceptance and commercial adoption.

2. Materials and methods

2.1. Experimental overview

The design used for this study is explained in Fig. 1. MCF (University of Maine Process Development Center, Orono, ME, USA) was purchased as an unmodified reference cellulose material alongside twelve industrially relevant surface-functionalized CNs. Each material underwent standardized sample dispersion and simulated gastrointestinal digestion [39,40]. Before and after digestion, samples were characterized using dynamic light scattering (DLS) and inductively coupled plasma-mass spectrometry (ICP-MS).

The CNs with functionalized surfaces were tested in a laboratory digestive system model composed of human intestinal epithelium Caco-2 cells, human colorectal adenocarcinoma mucus-producing HT-29 cells, and human Burkitt lymphoma Raji B cells [41]. The effects of CNs were assessed by examining cytotoxicity *via* membrane disruption, cytoplasmic membrane barrier integrity, cellular pro-inflammatory response, and cellular oxidative stress response at two different post-exposure periods (15 min and 4 h).

2.2. Surface-functionalized cellulose nanomaterials

Three representative chemical functionalities with varying reaction time and/or shear force were conducted to produce four levels of charges with respective dimensional attributes. Dissolving pulp was chemically modified by regio-selective C6 carboxylation by 2,2,6,6-tetramethylpyperidine-1-oxyl (TEMPO) mediated oxidation, C6 sulfation with chlorosulfonic acid, and C2, C3 carboxylation by sequential sodium

periodate-sodium chlorite (PC) oxidation followed by high-speed blending into respective functionalized CNFs, TCNFs, PCCNFs, and SCNF. The details related to the production and characterization of TCNF by TEMPO oxidation, SCNF by chlorosulfonic acid sulfation, and PCCNF by periodate-chlorite oxidation can be found in Jiang *et al* 2013 [42], Pingrey et al. 2022 [43], and Patterson et al. 2020 [44].

2.3. Preparation of cellulose suspensions

Each sample was weighed on an analytical balance (Mettler Toledo, Columbus, OH, USA) and transferred to a centrifuge tube. Ultrapure water (MilliQ 18.2 Ohms) was added to create a 2 % cellulose suspension for MFC, a 1 % cellulose suspension for the SCNFs, and a 0.6 % cellulose suspension for the TCNFs and PCCNFs (w/v) To ensure dispersion, each suspension was vortexed using a Vortex Genie 2 (Scientific Industries, Bohemia, NY, USA) for 10 min before testing as was previously reported [39,40]. The preparation method was determined to be the best dispersion technique for the cellulose materials [40]. Some analyses required additional dilutions, performed in cell culture medium unless otherwise stated.

2.4. Physical and chemical characterization of cellulose suspensions

Physical and chemical tests were conducted on the twelve cellulose suspensions. Dynamic light scattering with a Zetasizer Nanoseries Nano-ZS (Malvern Pananalytical, Almelo, Netherlands) was used to measure the hydrodynamic diameter (HDD), dispersity index (DI), and zeta potential (ζ potential). To ensure accuracy, the cellulose stock suspensions were diluted to 0.01 % with ultrapure water and placed in a disposable folded capillary cell DTS 1060 (Malvern Pananalytical, Almelo, Netherlands). For HDD and DI, each sample was scanned for 10 s, 11 times, in triplicate using a 173° backscatter angle in general-purpose mode. For zeta potential measurements, the Helmholtz–Smoluchowski model was used in the auto-report mode for 25 runs in triplicate for each sample. Each sample had a mean count rate >1000 counts per measurement to ensure accuracy [39]. Samples were run in triplicate.

2.5. Metal impurities

To prepare the samples, a hot block set at 95 °C was used along with a glass test tube containing 1 mL of each stock cellulose suspension. Concentrated nitric acid (HNO_3, 4 mL) was added to the vessel, and a plastic watch glass was placed over the top. After 1 h, the samples were removed and allowed to cool at room temperature. The samples were diluted with water to 25 mL. Then 50 μL of sample were added to 2 % HNO_3 and diluted to 10 mL. The sample digests were then placed in the autosampler and ran in triplicate along with an internal standard containing lithium, scandium, germanium, rhodium, indium, terbium, lutetium, and bismuth (Agilent, Santa Clara, CA, USA). Data acquisition and analysis were conducted using ICP-MS (Agilent 7900, Santa Clara, CA, USA) with MassHunter Software (Agilent). Samples were run in triplicate.

2.6. Preparation for toxicity testing

Cellulose samples were prepared at the following dose ranges *via* half-concentration serial dilutions: for MFC, the range was 2.0 %–0.2 % wt/vol; for SCNFs, the range was 1.0 %–0.2 % wt/vol; for TCNFs and PCCNFs, the range was 0.6 %–0.2 %. Dilutions were made using complete cell culture media (complete Dulbecco's Modified Eagle Medium/F-12 (Gibco)).

To test how human digestion affects the functionalized cellulose samples, they were subjected to three types of gastric fluids in sequence: salivary, gastric, and intestinal. This process, known as three-step gastrointestinal digestion, follows guidelines set by EFSA and mimics the chemical conditions, enzymes, and salts found in the mouth, stomach, and intestinal compartment. Each step of the digestion process was prepared separately, with an electrolyte solution and appropriate enzymes added to mimic the physiological conditions. The final concentrations of each component in the electrolyte solutions are listed in Supplemental Table 1. This information is based on research by Minekus et al. 2014 [39,45].

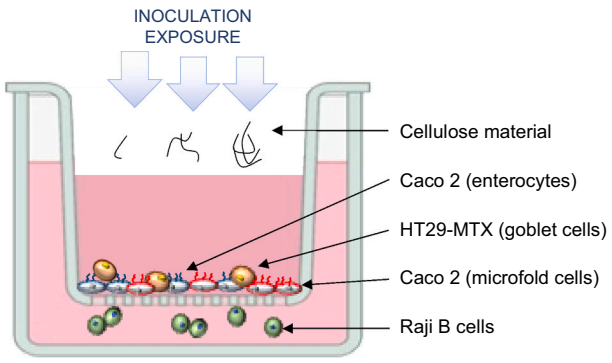

Fig. 2. The toxicological model used in these studies. Tri-culture assay progression is divided into 2 phases. Phase one is the gradual transition of the Raji B cells into media representative of the entire tri-culture model (apical and basolateral sides). Phase two includes differentiating Caco-2 cells (induced by Raji B cells) into M cells and adding mucus-producing HT29-MTX cells. The image below depicts the final assembled model used in these studies.

Simulated salivary fluid (SSF) was supplemented with human α-amylase (EC 3.2.1.1) to achieve a final concentration of 75 U/mL. Calcium chloride ($CaCl_2$) and ultrapure water were added to achieve a final concentration of 0.75 mM. Cellulose samples were subjected to this phase of digestion for 2 min at 37 °C with pre-warmed reagents. Simulated gastric fluid (SGF) was supplemented with porcine pepsin from gastric mucosa (EC 3.4.23.1) to achieve a final concentration of 2000 U/mL. Calcium chloride (0.075 mM) and phospholipids (0.17 mM) were added, and the fluid's pH was adjusted to 3.0 with hydrochloric acid (HCl). Cellulose samples previously undergoing the SSF digestion phase were subjected to this SGF, diluted by half (volume) with the gastric fluid, and incubated for 2 h at 37 °C with gentle shaking. Simulated intestinal fluid (SIF) was initially pH adjusted to 7.0 with sodium hydroxide (NaOH) and immediately followed by supplementation with pancreatin to achieve a final concentration of 100 U/mL (determined by trypsin activity assay), $CaCl_2$ (0.3 mM), and bile (10 mM). Cellulose samples previously undergone the SSF and SGF digestion phases were subjected to SIF, diluted by half (volume) with the intestinal fluid, and incubated for 4 h at 37 °C. All simulated digested samples were stored at −20 °C for up to 2 weeks.

2.7. Co-culture model assembly

The biological model used for this study has been described previously [46]. A depiction of the co-culture assembly is shown in Fig. 2. Each cell line was obtained from the American Type Culture Collection (ATCC) and maintained separately before co-culture. Human intestinal epithelium Caco-2 cells were utilized between passages 15–38, human colorectal adenocarcinoma mucus-producing HT29-MTX (HT-29) cells were utilized between passages 10–40, and human Burkitt lymphoma Raji B cells were utilized between passages 10–50 [46]. All cells were maintained in complete Dulbecco's Modified Eagle Medium/F-12 (Gibco) supplemented with 10 % heat-inactivated fetal bovine serum (Corning) and 1 % penicillin/streptomycin (Gibco) at a humidified 37 °C and 5 % CO_2 atmosphere until 70–80 % confluent. Passaging of cells was performed with 0.25 % Trypsin-EDTA (Invitrogen) and 1× PBS (Gibco).

The co-cultured cellular model was assembled in 12-well Transwell™ polystyrene plates (Corning) and PET inserts with a pore diameter of 0.4 μm (Corning 3460). Raji B, Caco-2, and HT-29 cell lines were

Table 1
Functionalized cellulose nanofibril (CNF) identifiers, reaction parameters, and attributes. For the sample identifiers (IDs), SCNF refers to sulfate-CNF, TCNF refers to TEMPO-CNF, and PCCNF refers to periodate-chlorite-CNF. The a, b, c, and d notations represent four different functionalities within each CNF series. The stock concentrations were 1 w/v% for SCNF and 0.6 w/v% for TCNF and PCCNF.

Sample ID	Reagent, concentration (mmol/g), time (min)	Blending time (min)	Charge (mmol/g)	Thickness (nm)	Width (nm)	Length (nm)
SCNFa	HSO_3Cl, 1, 30	30	1.49	1.2 ± 0.5 $n = 153$	3.2 ± 0.9 $n = 56$	693 ± 330 $n = 166$
SCNFb	HSO_3Cl, 1.25, 45	30	1.84	1.5 ± 0.4 $n = 250$	4.0 ± 1.0 $n = 73$	577 ± 294 $n = 175$
SCNFc	HSO_3Cl, 1.5, 60	5	2.23	1.5 ± 0.5 $n = 100$	3.2 ± 0.7 $n = 103$	501 ± 295 $n = 100$
SCNFd	HSO_3Cl, 1.5, 60	30	2.23	1.3 ± 0.3 n = 100	NA	365 ± 194 n = 100
TCNFa	NaClO, 3, 30	30	1.10	1.6 ± 0.9 n = 100	6.5 ± 2.2 $n = 50$	551 ± 200 n = 50
TCNFb	NaClO, 5, 50	10	1.42	1.7 ± 0.7 n = 100	6.1 ± 1.6 $n = 47$	486 ± 174 n = 50
TCNFc	NaClO, 5, 60	30	1.42	1.3 ± 0.7 n = 100	4.6 ± 1.6 $n = 30$	530 ± 145 n = 50
TCNFd	NaClO, 8, 80	30	1.48	1.8 ± 0.7 n = 100	4.9 ± 2.0 n = 50	486 ± 206 n = 50
PCCNFa	$NaIO_4$, 3.08, 4; $NaClO_2$, 6.16, 30	30	0.72	2.7 ± 0.9 $n = 37$	5.9 ± 1.6 n = 50	452 ± 162 n = 30
PCCNFb	$NaIO_4$, 3.08,4 $NaClO_2$, 6.16, 9 h	30	0.82	2.5 ± 1.2 $n = 52$	5.7 ± 1.6 n = 47	533 ± 275 n = 30
PCCNFc	$NaIO_4$, 3.08, 4; $NaClO_2$, 6.16, 12 h	30	0.91	2.4 ± 1.1 n = 30	5.5 ± 1.6 n = 30	381 ± 150 n = 30
PCCNFd	$NaIO_4$, 4.62, 4; $NaClO_2$, 6.16, 6 h	30	1.04	2.1 ± 0.9 n = 30	5.6 ± 1.7 n = 50	344 ± 170 n = 30

plated in a 9:9:1 ratio, respectively, with 1.5×10^4 Raji B cells in the basolateral compartment and 1.5×10^4 Caco-2 cells in the apical chamber. Initial plating of only Raji B and Caco-2 cells for approximately 5 days allowed for a sub-population of Caco-2 cells to differentiate into microfold cells (M-cells) before adding mucous-producing HT-29 cells. After differentiation, HT-29 cells were layered in the apical chamber at the ratio noted. The characterization of this advanced intestinal co-culture has been previously reported [39,47].

$$\%\text{Cytotoxicity} = \left[\frac{\text{Cellulose exposure LDH activity} - \text{Spontaneous LDH activity}}{\text{Maximum LDH activity} - \text{Spontaneous LDH activity}}\right] \times 100$$

2.8. Cellulose exposure to cellular model

Digested cellulose samples were resuspended in fresh warmed media and added to the apical chamber of 12-well Transwell plates, replacing aspirated media after 24 h post-HT-29 cell plating. Exposed plates were incubated at humidified 37 °C and 5 % CO_2 atmosphere for either 15 min or 4 h. Cell supernatant was collected for the lactate dehydrogenase (LDH) assay. In contrast, cells were harvested and lysed for interleukin-6 (IL-6) and glutathione reductase (GR) assay detection. Vehicle controls included ultrapure deionized water and simulated gastric fluid (without cellulose). Positive controls were 1 % (v/v) Triton X-100 (Amresco, Solon, OH, USA) and 1 μM phorbol myristate acetate (PMA, Thermo) to elicit GR and IL-6 responses, respectively.

2.9. Cytotoxicity via membrane disruption

The concentration of lactate dehydrogenase (LDH) in tri-culture supernatant after digested cellulose exposure was quantified using CyQUANT LDH Cytotoxicity Assay kit (Invitrogen C20301). A 1× LDH positive (reaction) control was run parallel to Triton X-100 positive control. Sterile ultrapure water was used to quantify spontaneous LDH activity, and 10× lysis buffer was added to quantify the maximum LDH activity per kit recommendations. After post-exposure periods, the apical chamber supernatant was transferred to a 96-well flat-bottom plate (Thermo) in triplicate. The reaction mixture and stop solution were added to wells according to the assay kit, and absorbance was measured at 490 and 680 nm on a Biotek Epoch2 microplate reader. Percent (%) cytotoxicity was calculated for each well using the following equation:

2.10. Cytoplasmic membrane barrier integrity

Transepithelial electrical resistance (TEER) measurements were taken with an EVOM3 and STX2-PLUS electrode (World Precision Instruments Sarasota, Florida) on 12-well Transwell plates seeded with cells as noted previously. Complete tri-cultures were allowed to incubate for 24 h before TEER testing. Measurements were taken at three locations in each Transwell insert and experiments were performed in triplicate. Plates were allowed to equilibrate at room temperature for 15 min before TEER testing to reduce variability in resistance measurements due to changing CO_2 levels and temperature drift. TEER values were calculated by multiplying the resistance (in ohms) by the area of the Transwell insert (1.12 cm^2).

2.11. Cellular pro-inflammatory response

Pro-inflammatory response marker IL-6 was quantified in pg/mL in cellulose-exposed cell lysates using an Enzyme-Linked Immunosorbent Assay (ELISA, BMS213–2, Invitrogen, Waltham, MA). Briefly, digested cellulose samples were added to the apical chamber for 15 min and 4 h at humidified 37 °C and 5 % CO_2 atmosphere after which supernatant was removed. The basolateral chamber was aspirated and discarded for ease of lysing Caco-2 and HT-29 cells. Cells in the apical chamber were

Table 2
Characterization of the twelve surface-functionalized and unmodified MFC. The table reports the average hydrodynamic diameter (HDD) ± the standard deviation, dispersity index (DI) ± the standard deviation, and zeta potential (ZP) ± the standard deviation for samples in ultrapure water *vs* after simulated digestion.

Sample ID	In ultrapure water			After simulated digestion		
	HDD (nm)	DI (unitless)	ZP (mV)	HDD (nm)	DI (unitless)	ZP (mV)
MFC	14,410 ± 1047	0.827 ± 0.16	−33 ± 0.945	977.4 ± 154.6	0.750 ± 0.068	−25.2 ± 0.321
SCNFa	846.6 ± 250.9	0.965 ± 0.061	−61.2 ± 6.59	436.5 ± 32.48	0.453 ± 0.052	−39.1 ± 2.12
SCNFb	1172 ± 322.2	0.978 ± 0.038	−36.6 ± 3.66	403.2 ± 17.5	0.498 ± 0.032	−46.2 ± 0.265
SCNFc	478.2 ± 82.55	0.792 ± 0.103	−48.7 ± 1.32	771.5 ± 21.38	0.522 ± 0.007	−43.4 ± 0.757
SCNFd	817.1 ± 22.42	0.825 ± 0.05	-43.4 ± 1.56	789.1 ± 80.96	0.601 ± 0.037	−36.6 ± 2.02
TCNFa	1448 ± 217.3	0.980 ± 0.035	−60.9 ± 3.74	522.3 ± 23.52	0.526 ± 0.123	−38.8 ± 1.42
TCNFb	1163 ± 167.4	1.000 ± 0	−53.9 ± 0.643	489.3 ± 63.23	0.551 ± 0.05	−37.9 ± 1.25
TCNFc	602.4 ± 40.6	0.886 ± 0.054	−57.3 ± 1.89	477.5 ± 51.43	0.602 ± 0.02	−39.6 ± 1.42
TCNFd	625.6 ± 53.75	0.867 ± 0.084	−53.2 ± 3.57	455.7 ± 35.29	0.540 ± 0.029	−41.6 ± 0.643
PCCNFa	247.5 ± 1.484	0.449 ± 0.004	-53.6 ± 0.4	814.4 ± 54.53	0.701 ± 0.108	−39.7 ± 2.32
PCCNFb	741.8 ± 9.877	0.548 ± 0.026	-50.4 ± 3.35	745.3 ± 44.91	0.561 ± 0.056	−42.4 ± 1.29
PCCNFc	531.7 ± 17.33	0.801 ± 0.209	−50.6 ± 0.306	731.4 ± 37.55	0.566 ± 0.039	-37.7 ± 1.37
PCCNFd	1275 ± 61.85	0.641 ± 0.02	-50.5 ± 0.907	821.8 ± 166.5	0.631 ± 0.085	−41.7 ± 1.71

washed 2X with cold sterile 1X PBS (Gibco). Transwell inserts were treated with cold RIPA lysis and extraction buffer (Thermo) and allowed to sit on ice for 10 min. The cell lysate was collected in 1 mL microcentrifuge tubes and centrifuged for 10 min at 12,000 x RPM at 15 °C (Eppendorf 5810). The pellet was discarded, and the supernatant was stored at −80 °C until use [39,48].

2.12. Cellular oxidative stress response

Glutathione reductase (GR) activity, an indicator of oxidative stress, was measured fluorescently utilizing an immunoactivity kit (Invitrogen EIAGRF). Hydrogen peroxide (H_2O_2), a known inducer of oxidative stress, was used as a positive control. Lysate was collected with RIPA buffer on ice and measured for GR activity per the manufacturer's protocol. Fluorescence was read at excitation and emission wavelengths of 390 and 510 nm, respectively. Data was analyzed utilizing a four-parameter curve.

2.13. Statistical analyses

Pairwise differences were determined using analysis of ordinary one-way ANOVA and a two-sample *t*-test assuming equal variance. All statistical analyses were performed in Prism 8.3.0 (GraphPad, San Diego, CA, USA). The study included three replicates performed in triplicate (n of 9) for the biochemical assays.

A thorough 2-step statistical analysis was conducted to analyze the LDH, IL-6, and GR data sets. First, the slope values of each cellulose were compared with their respective controls. Then, the estimates were evaluated along with the confidence interval. The slope value estimates translate to a measure of the sensitivity of the response. The further the value is from the vertical line, the more sensitive the cells are to cellulose's dose. In step 2, the mean values of each cellulose were compared with their respective controls and plotted as estimates of confidence. The mean value estimates translate to a measure of the potency of the response. The further the value is from the vertical line, the more sensitive the cells are to the biological endpoint.

3. Results and discussion

3.1. Cellulose physical and chemical characterization

The three-chemical functionalization of C6 carboxylation (R-COOH), C6 sulfation (R-SO_2OH), and C2, C3 carboxylation (R-COOH) was conducted under varied reagent to cellulose molar ratios and lengths of time followed by blending provided widest extents of reaction range, denoted by 3–4 levels of charges, and nanofibril dimensions (Table 1). SCNF series exhibited the highest charge, averaging −1.95, followed by the TCNF series at −1.36 and the PCCNF series at −0.873. Furthermore, it was observed that the length of individual fibrils decreased for the SCNF and PCCNF series as reaction time and blending time increased whereas TCNF showed no clear trend with respect to rection and blending variables. Closer observation of nanofibril morphology showed more individualized SCNF and TCNF and consistently more heterogeneous PCCNF fibril dimensions (Fig. 3). The varied productivities of these three reactions and blending process were also evident by the CNF yields in the supernatant (centrifugation 5000 RPM, 15 min) in the order of highest yielding sulfation (99 to 100 %), then TEMPO oxidation (82.1 to 100 %), and PC oxidation (49.3 to 100 %). These three properties (fibril surface functionality, charge, and length) can be related to the observed toxicological outcomes. Lastly, no trace metals were detected in any samples.

The twelve surface-functionalized CNs and unmodified MFC were analyzed after suspension in ultrapure water and exposure to a simulated 3-phase digestion fluid. The unmodified MFC measured at 14,400 nm in water. Each surface functionalization produced measurements of varying sizes, with TEMPO oxidation producing the largest values, followed by periodate-chlorite oxidation and sulfonation. All thirteen CN samples showed high polydispersity when suspended in water. The zeta potential measurements indicated the surface charge of fibril agglomerate in suspension, with TEMPO oxidation producing the most negative zeta potential, followed by periodate-chlorite oxidation and sulfonation. However, when comparing the CN samples suspended in water to the same materials suspended in simulated digestion fluid, many hydrodynamic diameters and dispersity indices decreased. Additionally, the zeta potential measurements became less negative. Digesting the CNs before inoculation to cells altered some physicochemical properties consistent with other published reports [37–39,49,50].

3.2. Cytotoxicity assessment

We performed a cytotoxicity evaluation using an intestinal cell model to assess its response to CNs in simulated digestion fluid, Fig. 4. The test measures lactate dehydrogenase (LDH) cytoplasmic enzyme activity, which increases after plasma membrane damage due to apoptosis or necrosis. We tested different cellulose concentrations and normalized the LDH activity to a standard. Pairwise differences were determined using analysis of ordinary one-way ANOVA and a two-sample *t*-test assuming equal variance. The results showed that none of the cellulose treatments caused significant cytotoxic responses

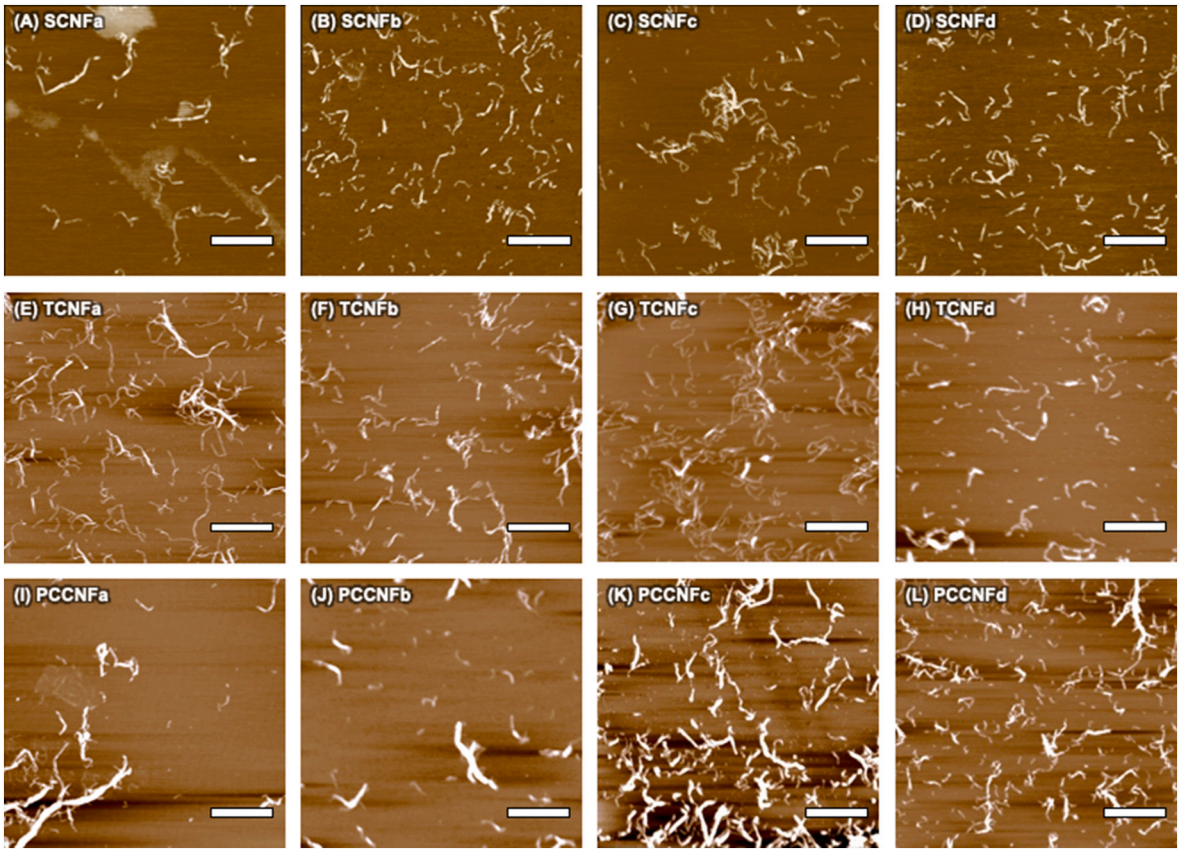

Fig. 3. The atomic force microscopy (AFM) images of three functionalized cellulose nanofibrils. Asylum Research MFP-3D AFM was used with OMCL-AC160TS standard silicon probes with a nominal tip radius of 7 nm and a spring constant of 26 N/m. To collect surface profiles, a few drops of diluted SCNF dispersion (approximately 0.0001 wt%) were placed on freshly cleaved mica discs, allowed to dry, and then analyzed under ambient conditions using tapping mode. The scale bar is 1 μm.

compared to untreated or vehicle controls.

In addition to assessing the LDH activity, we analyzed the data to determine if the cellular response to cellulose exposure differs among the treatments (Fig. 5). This analysis was performed by comparing the confidence interval overlaps of the mean values. Responses were noted as different when the value did not overlap with the CI of the untreated cells (UT). Pairwise differences were determined using analysis of variance (ANOVA) and Tukey's Honestly Significant differences (HSD) test. Furthermore, we investigated whether the cellular response to cellulose differs among exposure concentrations within the same treatment. This analysis compared the confidence interval overlaps of the slope values from a linear model with untreated cells (UT) as a reference group. Responses were noted as different from UT when the value did not overlap with 0.

Results from the confidence interval analyses of the mean (*i.e.,* potency) for the LDH activity assays showed that the positive control was statistically significant for the 15-minute and 4-hour time points. Analyses of slope (*i.e.,* sensitivity to cellulose treatments/type across dose) for the LDH activity assays showed that only the positive control (Triton X) was statistically significant for the 15-minute exposure timepoint.

3.3. Gastrointestinal barrier integrity impairment

Next, we assessed the effects of surface-functionalized CNs on cellular barrier integrity using transepithelial electrical resistance (TEER) (Fig. 6). TEER values indicate membrane barrier integrity in endothelial/epithelial cell layers. The gastrointestinal tract's epithelial layer acts as a barrier to underlying tissues. Therefore, disruption of this membrane could lead to unwanted health effects, adding to the toxicological profile of compounds studied. Barrier integrity and tight junction stability are regarded as indicators that correlate between *in vitro* to *in vivo* models [51–53]. A decrease in resistance indicates decreased barrier integrity and cytoplasmic membrane disruption. Daily post-exposure measurements for eight days indicated a steady increase in electrical resistance; linear regression was used to model the data. The untreated control cells (UT) exhibited 390–450 Ω cm^2 readings on day 8, whereas the positive control exhibited 170–205 Ω cm^2 readings. Across the three cellulose functionalization types (*i.e.,* SCNFs, TCNFs, and PCCNFs), we observed that as the functionalization density and charge increased, the cellular barrier resistance of exposed cells decreased. Statistically, three of the four PCCNFs, two of the four TCNFs and one of the SCNFs significantly reduced barrier integrity compared to the untreated sample at day 8 post-exposure (Fig. 6E).

Further analyses included a comparison of a linear fit slope. There was little change in slope among the 12 functionalized CNs, but many CNs induced lower resistance compared to the untreated slope. Estimates indicate deviation of treatment slope from untreated slope (Fig. 6F gray shaded area) and from vehicle control (blue shaded area). While there was greater overlap of confidence intervals upon the comparison of treated slopes to untreated slopes than to vehicle control, all values fall within the two controls except for the positive control and MCF.

3.4. Pro-inflammatory response

We measured the impact of surface-functionalized CNs on the inflammatory response of gut cells (Fig. 7). An ELISA was utilized to determine the pro-inflammatory cytokine interleukin 6 (IL-6) produced

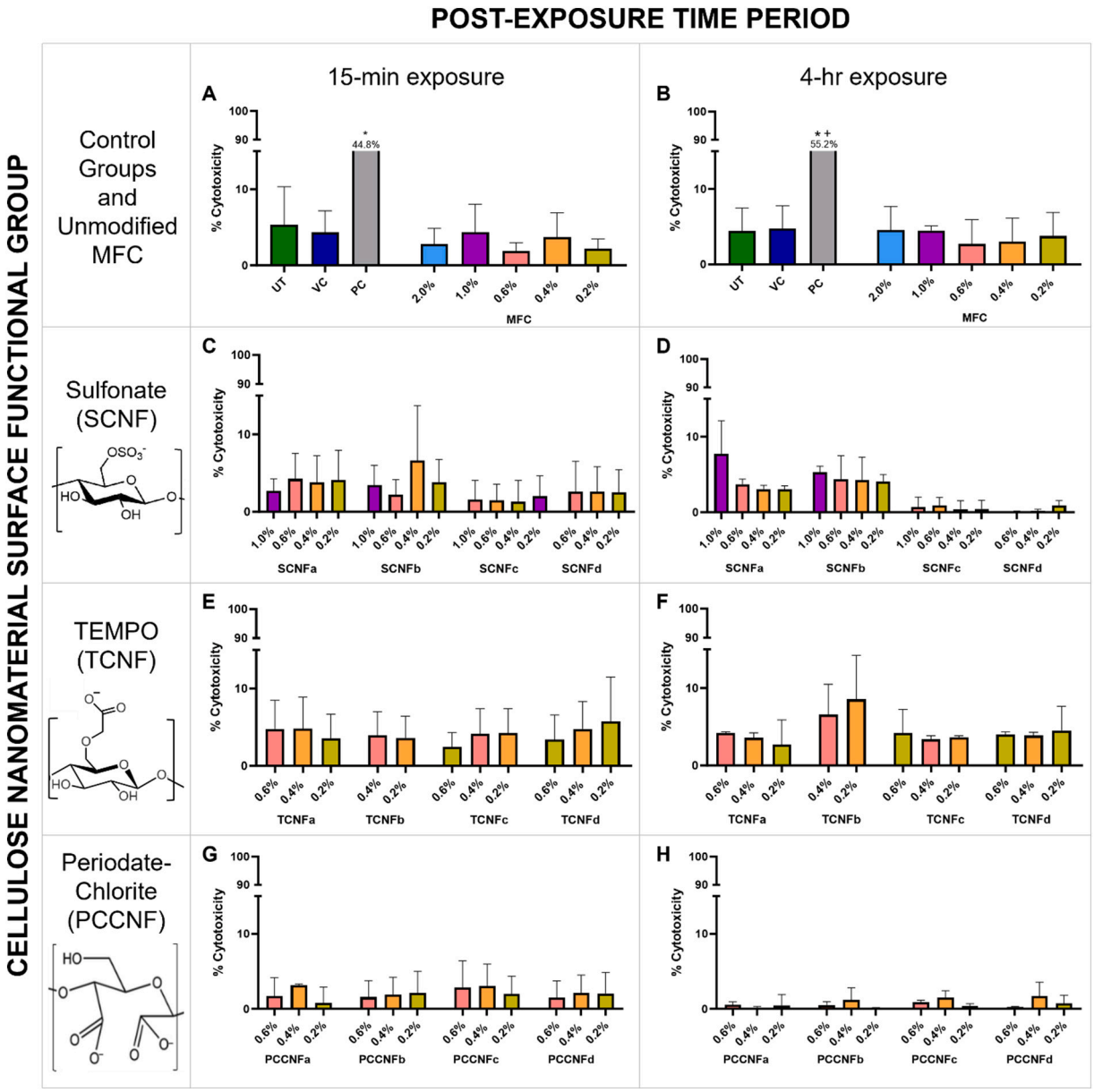

Fig. 4. The cytotoxicity induced after exposure to digested surface-functionalized cellulose nanomaterials in the co-cultured gastrointestinal *in vitro* model was measured by lactate dehydrogenase (LDH). LDH values were normalized to untreated control cell populations and expressed at.% cytotoxicity. The first column includes data collected after the 15-minute post-exposure period, and the second column includes data collected after the 4-hr post-exposure period. Individual graphs include (A and B) controls [untreated cells (UT), simulated gastrointestinal fluid (VC: vehicle control), and 1 % (v/v) Triton X-100 (PC: positive control), and unmodified cellulose material (MFC: unmodified cellulose fiber)]; (C and D) sulfonate surface-functionalized CNs (SCNF); (E and F) TEMPO surface-functionalized CNs (TCNF); (G and H) periodate-chlorite surface-functionalized CNs (PCCNF). Significance was defined where $^{*}P < 0.05$ for untreated cells compared to CN exposures. +P 0.05 for vehicle control cells compared to CN exposures. Values include three replicates performed in triplicate ($n = 9$).

by the cells. IL-6 activity was normalized to untreated cells, and comparisons were made for the 12 functionalized CNs to the untreated cells and the vehicle control. Most of the unmodified (MFC) samples caused a significant difference in IL-6 levels compared to UT.

In contrast, approximately half of the 15-minute and none of the 4-hour exposures were significant compared to the VC. In the SCNF series, 15-minute exposure exhibited more significant effects on IL-6 levels than 4-hour exposure. Conversely, within the TCNF series, 4 h of exposure resulted in more significant effects than 15 min. Similar effects were observed in the PCCNF series for both durations of exposure. Overall, treatments exhibited more significant effects within a 15-minute exposure period than a 4-hour exposure period compared to the VC.

In addition to reporting the IL-6 expression, an analysis was conducted to determine whether the cellular response to cellulose exposure differs among the treatments (Fig. 8). The means (*i.e.,* potency) and slopes (*i.e.,* sensitivity) for surface-functionalized CN treatments were compared. Means were not considered statistically different from UT if they overlapped with 1 and not statistically different from VC if they overlapped with the VC range (shaded blue). Slopes were not considered statistically significant if overlapped with 0 (UT).

Results from the confidence interval analysis of IL-6 mean (*i.e.,* the potency of treatment) found that the following treatments were statistically significant upon comparison to UT: MFC, SCNFa, and PCCNFa for 15 min; SCNFa, SCNFc, TCNFa, TCNFb, TCNFc, and PCCNFa at 4 h. Comparing the IL-6 mean to VC, none of the cellulose treatments were significant. Results from the confidence interval analysis of IL-6 slope (*i.e.,* sensitivity to treatment across dose) found that only TCNF at 4-hour exposure was significant.

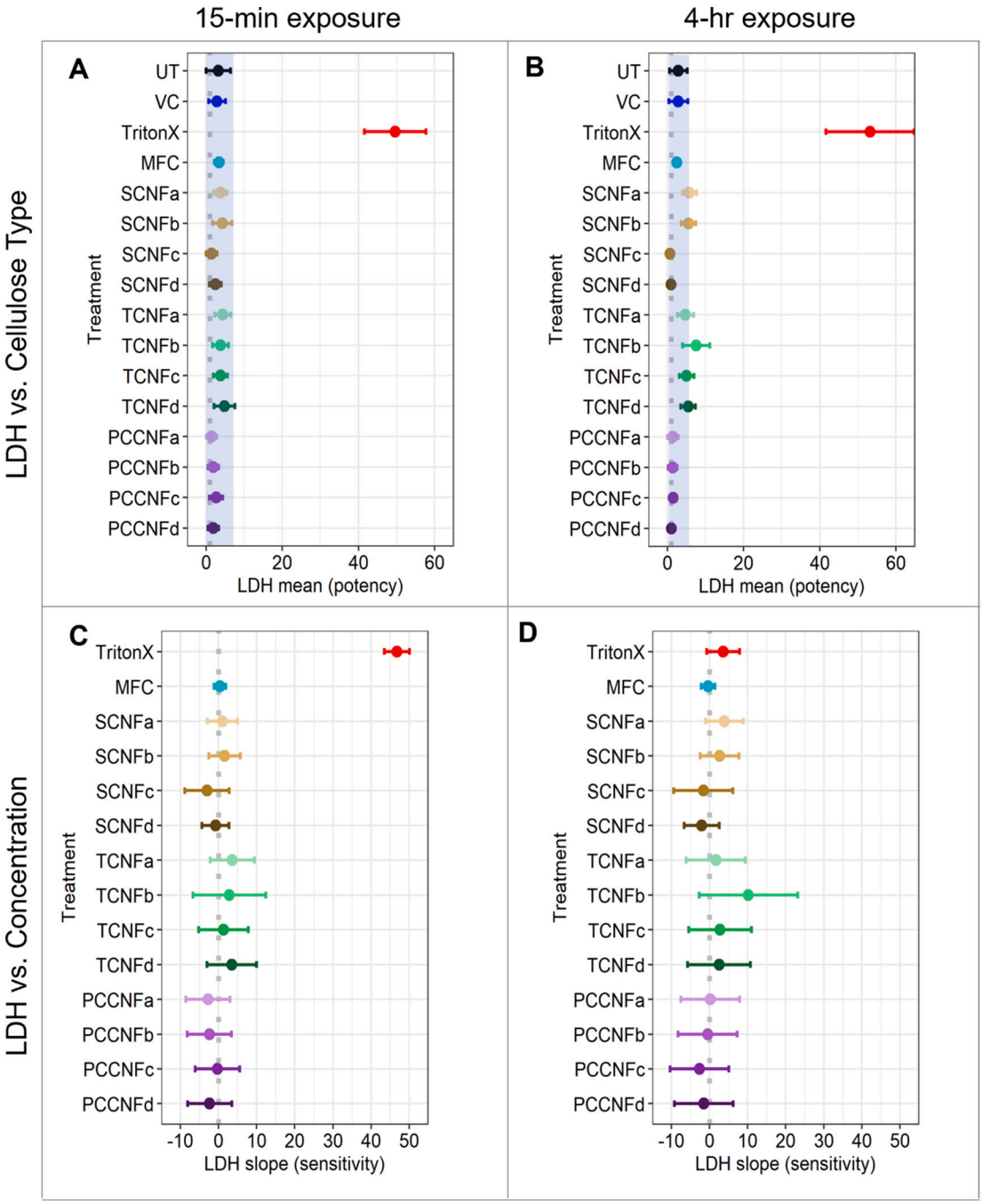

Fig. 5. LDH mean and slope estimates with 95 % confidence intervals (normalized to LDH standard). (A-B) LDH mean *vs.* cellulose type (potency); intervals that overlap with UT are not significantly different (cannot reject the null hypothesis); significant: Triton X at 15 min and 4 h. The shaded blue bar indicates the vehicle control (VC) comparison range (C—D) LDH slope (change over concentration) *vs.* cellulose type (sensitivity) from the linear model with UT as the reference group; intervals that contain 0 (intersecting the dotted line) are not significantly different (cannot reject the null hypothesis); significant: Triton X at 15 min.

3.5. Oxidative stress assessment

The influence of surface-functionalized CNs on the oxidative stress response of intestinal cells was assessed *via* a glutathione reductase fluorescent activity kit, which measured the levels of glutathione reductase (GR), an antioxidant enzyme produced by the cells. Results (Fig. 9) were normalized to untreated cells and compared to the UT and VC for significance.

GR increased slightly in the unmodified MFC series as MFC concentration decreased for 15-min exposures, where most were statistically significant compared to UT but not to VC. MFC 4 h exposure did not elicit a significant overall response in GR, and there was no discernible trend. In the SCNF series, a noticeable decrease was observed after 15 min from SCNFa-d, with SCNFa exhibiting statistical significance compared to UT across all doses. Although only a few TCNF materials exhibited effects following a 15-minute exposure, many 4-hour exposures showed statistical significance compared to the untreated (UT) and vehicle control (VC) groups. Similarly, in the PCCNF series, PCCNFa, was more significant compared to UT and VC after 4 h.

In addition to reporting the glutathione reductase expression, an analysis of the mean and slope of CN exposures was conducted to determine whether the cellular response to cellulose exposure differs among the treatments (Fig. 10). Results from the confidence interval analysis of GR mean (*i.e.,* the potency of treatment) found the following

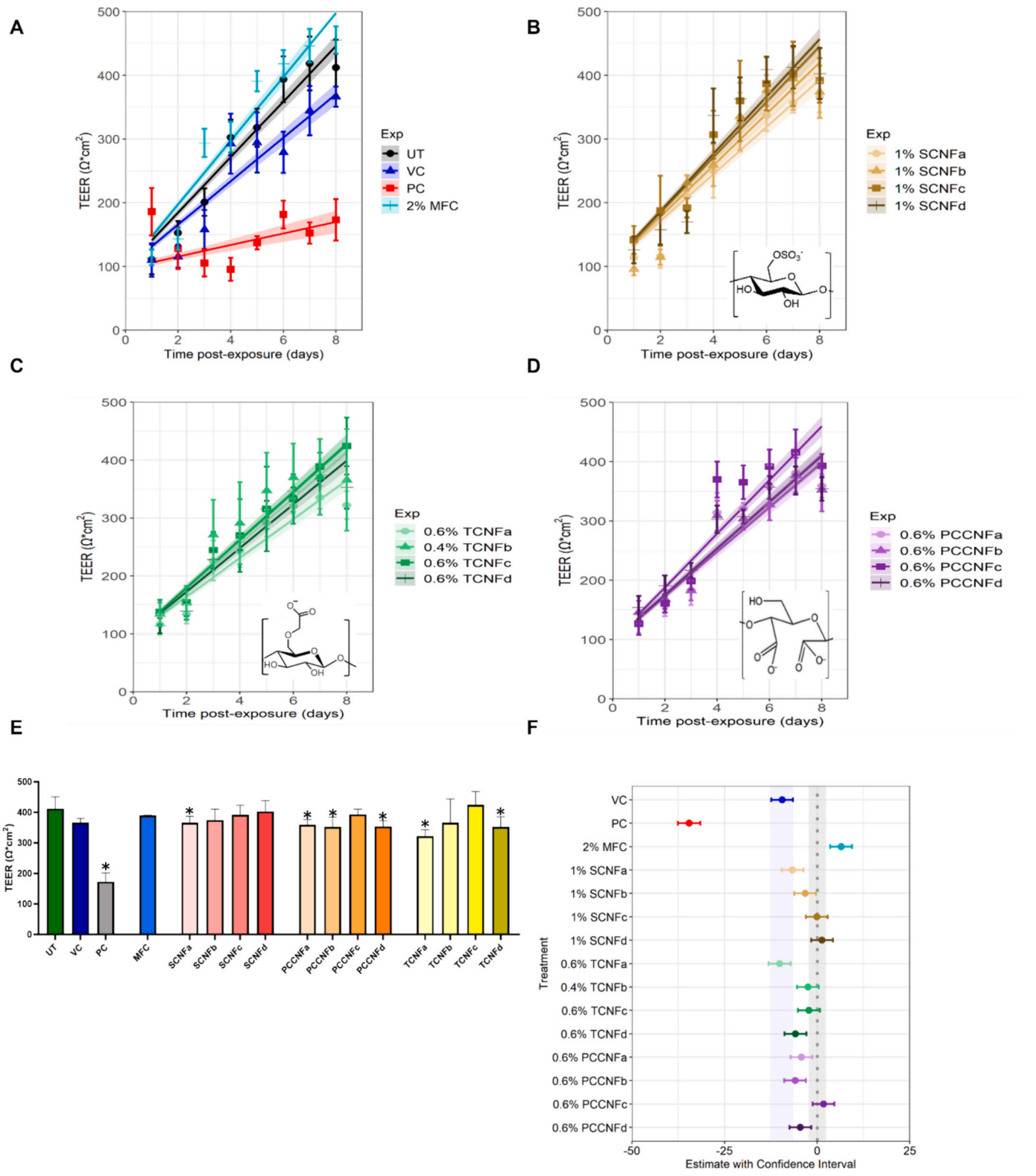

Fig. 6. The barrier integrity of an *in vitro* gastrointestinal co-culture model after exposure to digested surface-functionalized cellulose nanomaterials, as measured by transepithelial electrical resistance (TEER, Ω cm^2). TEER is plotted *vs.* time for (A) control samples [untreated cells (UT), simulated gastrointestinal fluid (VC: vehicle control), 1 mM phorbol myristate acetate (PMA, PC: positive control), and unmodified cellulose material [MFC: cellulose fiber, 2 %]; (B) the sulfonate surface-functionalized CNs [SCNF a-d]; (C) the TEMPO surface-functionalized CNs [TCNF a-d]; (D) the periodate-chlorite surface-functionalized CNs [PCCNF a-d]. (E) A comparison of each CN treatment at 8 days post-exposure [$*p < 0.05$ for treatment *vs* UT]. (F) The slope estimates with 95 % confidence intervals from linear regression, with UT as a reference group (gray shaded). Light blue shading is the confidence interval for the vehicle control.

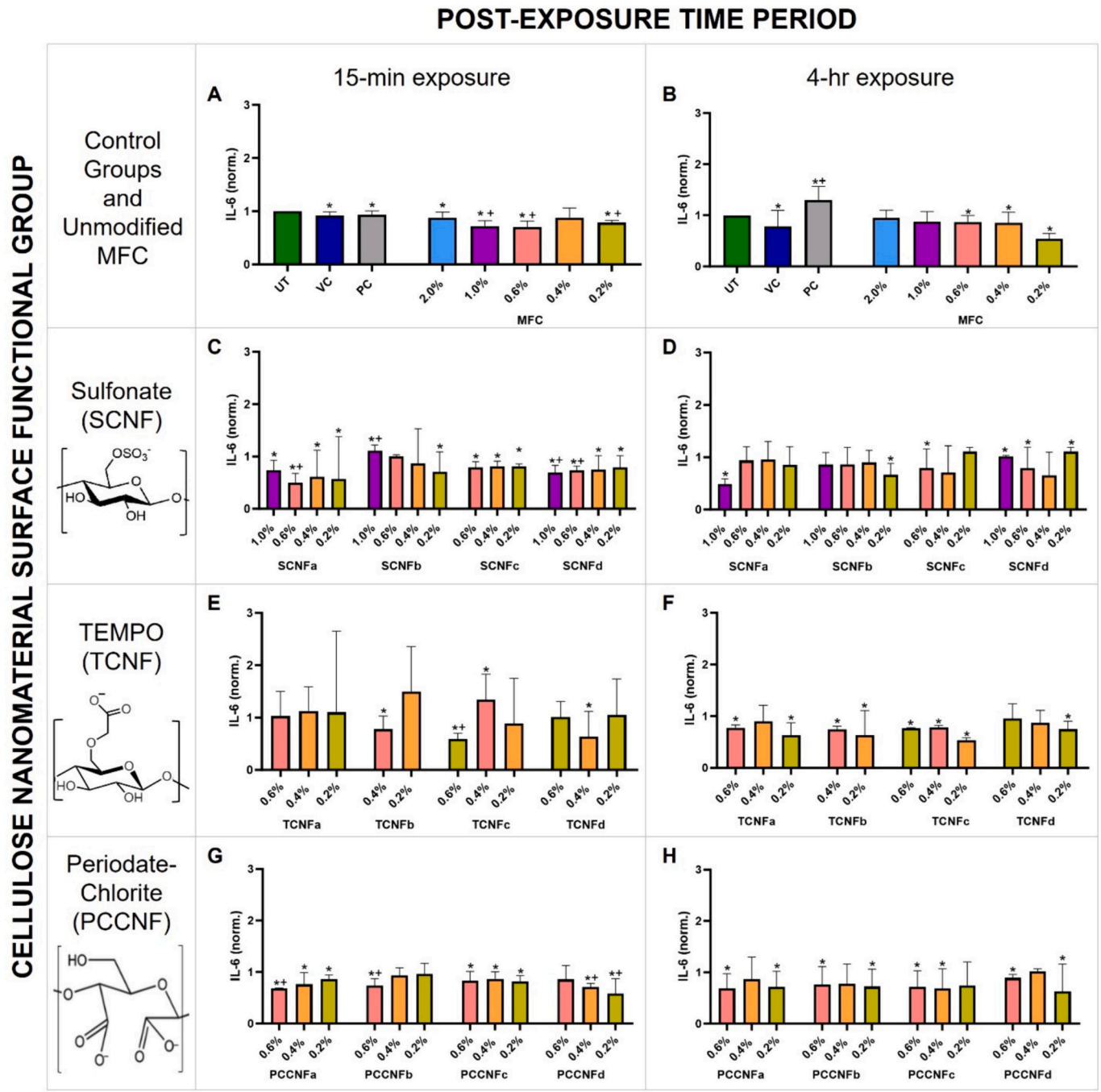

Fig. 7. The cellular pro-inflammatory response of digested surface-functionalized cellulose nanomaterials co-cultured gastrointestinal *in vitro* model measured by interleukin 6 (IL-6). IL-6 values were normalized to untreated control cell populations. The left panel includes data collected after a 15-minute post-exposure period, and the right panel includes data collected after a 4-hour post-exposure period. Individual graphs include (A and F) controls [untreated cells (UT), simulated gastrointestinal fluid (VC: vehicle control), and 1 mM phorbol myristate acetate (PMA, PC: positive control)]; (B and G) unmodified cellulose material [MFC: microfibrillated cellulose]; (C and H) sulfonate surface-functionalized CNs [SCNF]; (D and I) TEMPO surface-functionalized CNs [TCNF]; (E and J) periodate-chlorite surface-functionalized CNs [PCCNF]. *$P < 0.05$ for untreated cells compared to CN exposures. + $P < 0.05$ for vehicle control treated cells compared to CN exposures. Values include three replicates performed in triplicate ($n = 9$).

treatments were statistically significant to UT: Triton X, SCNFa, SCNFb, and TCNFd for 15 min; Triton X, SCNFb, SCNFc, SCNFd, TCNFa, TCNFb, TCNFc, and TCNFd for 4 h. Comparison of GR mean to VC reduced the significant differences to Triton X, SCNFa for 15 min and Triton X, SCNFb, TCNFa, TCNFb, TCNFc, and TCNFd for 4 h exposure. There is less significance when responses are compared to the simulated digestive fluid (VC) effect than to the untreated cells. Results from the confidence interval analysis of GR slope (*i.e.,* sensitivity to treatment across dose) found the following treatments were statistically significant: Triton X for the 15-minute exposure; SCNFa, TCNFa, and TCNFd for 4-hour exposures.

This study highlights some challenges when performing toxicity screening of functionalized cellulose fibrils. First, cellulose fibrils may aggregate or agglomerate in cell culture media, and characterizing the degree of agglomeration is difficult [54]. Second, the absorption capacity varies for each type of cellulose moiety, and the increase in

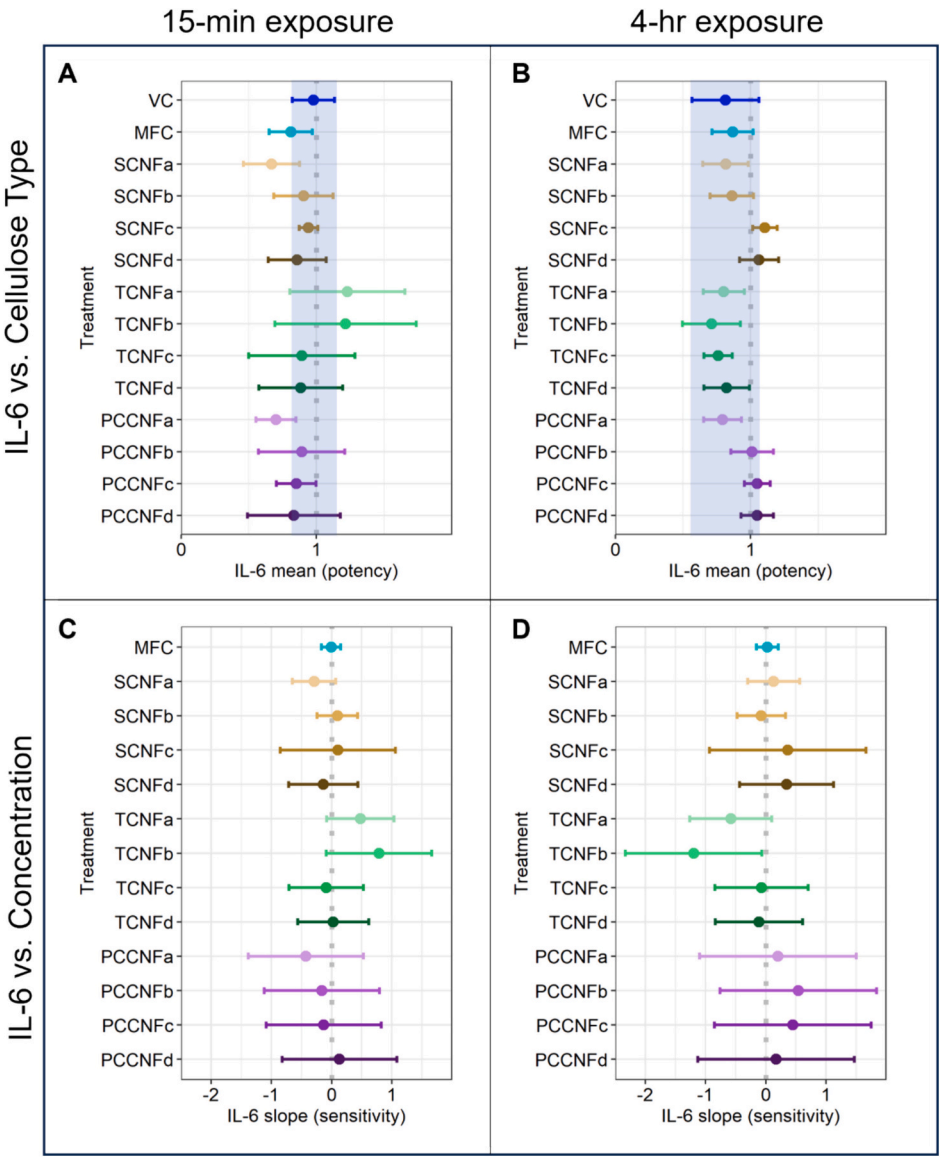

Fig. 8. IL-6 mean and slope estimates with 95 % confidence intervals were normalized to untreated cells (UT). (A-B) Mean IL-6 activity for 15-minute and 4-hour exposure; intervals that contain 1 (intersecting the dotted line) are not significantly different from UT. The shaded blue bar indicates the VC comparison range. (C—D) The slope of IL-6 activity over dose *vs* cellulose type for 15 min and 4 h of exposure; intervals that contain 0 (intersecting the dotted line) are not significantly different from UT.

physicochemical properties can promote adduct formation [55]. Third, as the acute studies did not yield significant results for the tested endpoints, we propose evaluating other toxicological endpoints over longer exposure periods [56].

While challenges have been identified, we also cite distinct advantages in the model used and data collected. First, our method was precisely designed to investigate high-level effects through a high-throughput screening assay [46]. Second, the design provides the ease and ability to test a wide range of cellulose compounds in a manner that better represents a human gut model; specifically, the addition of multiple cell layers in the model produces a biologically relevant condition for exposure. Third, simulated gastrointestinal digestion allows us to see how the cellulose moieties are modified chemically and physically before cell exposure. EFSA and other researchers acknowledge that the simulated digestion process is an acceptable approach for screening level testing of food ingredients [39].

The results of this study reveal the strategy needed to continue functionalized cellulose environmental health and safety research in the immediate future. Comparing a positively charged cellulose moiety to the negatively charged versions tested presently and extending the exposure periods from acute to chronic will help decipher absorption and distribution properties *in vivo* and adsorption, adduct formation, and uptake properties *in vitro*. Additional data exploring the downstream molecular effects are also needed [57–60].

This study examined how surface chemistry impacts toxicity by combining two important endeavors: standardized methods for physicochemical characterization and utilization of a standard alternative testing protocol for diverse CNs, including unmodified MFC and surface-functionalized materials. The synthesized CNs with tailored differences in physical and chemical properties (surface chemistry, charge density, morphology) were evaluated for induced toxicological responses (Table 3). The effects of different doses and post-exposure times of cellulose products on an *in vitro* model were monitored. Data collected from these experiments provide a comprehensive overview of the potential toxicological effects of CNs on the gastrointestinal system *via* the ingestion exposure route.

For the potency analyses, the effects of the exposure groups that included a cellulose material were compared to those of the untreated,

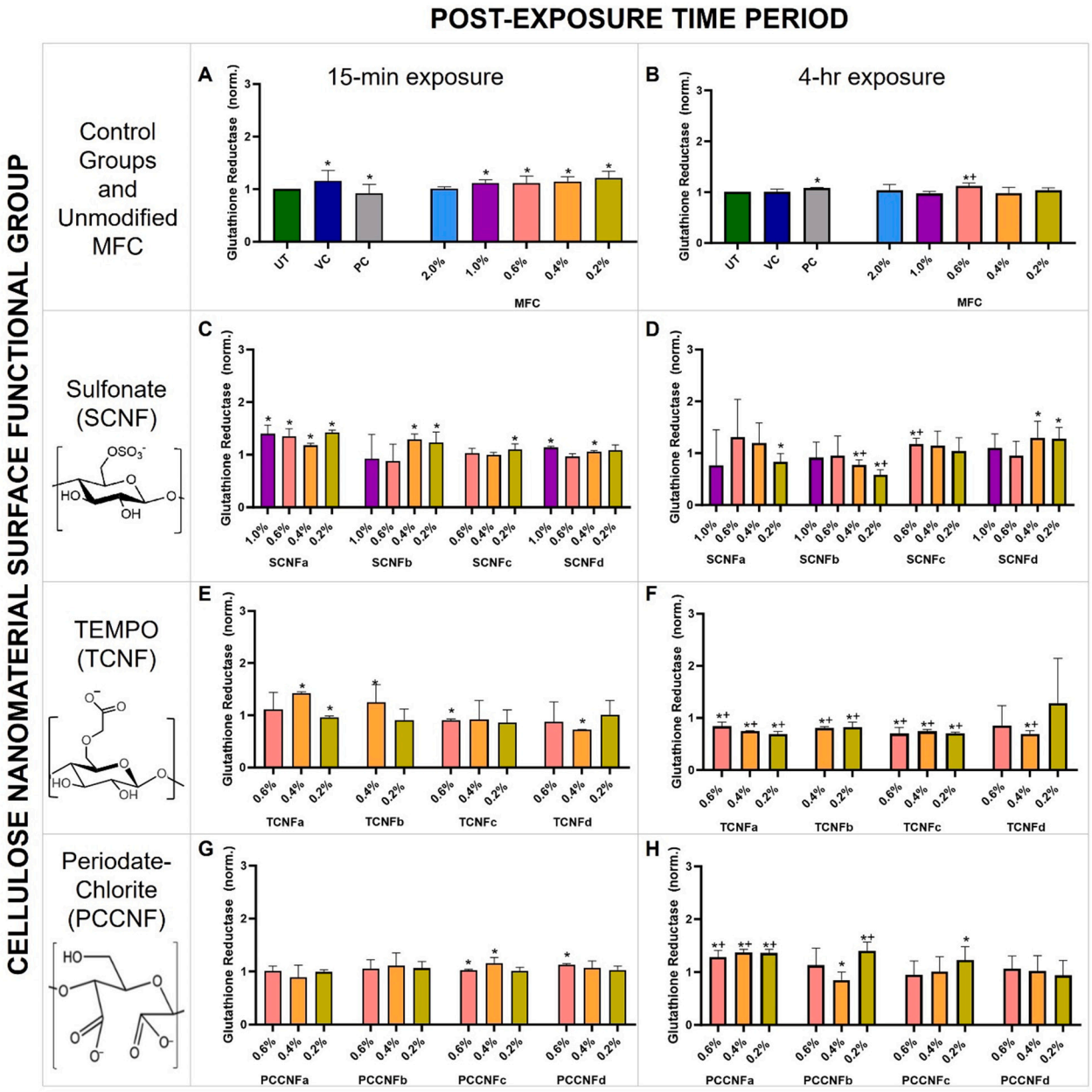

Fig. 9. The cellular oxidative stress response of digested surface-functionalized cellulose nanomaterials co-cultured gastrointestinal *in vitro* model measured by glutathione reductase (GR). GR values were normalized to untreated control cell populations. The left panel includes data collected after 15 15-minute post-exposure period, and the right panel includes data collected after 4-hour post-exposure period. Individual graphs include (A and F) controls [untreated cells (UT), simulated gastrointestinal fluid (VC: vehicle control), and 1 % (v/v) Triton X100 (PC: positive control)]; (B and G) unmodified microfibrillated cellulose [MFC]; (C and H) sulfonate surface-functionalized CNs [SCNF]; (D and I) TEMPO surface-functionalized CNs [TCNF]; (E and J) periodate-chlorite surface-functionalized CNs [PCCNF]. Significance was defined where $*P < 0.05$ for untreated cells compared to CN exposures. + P < 0.05 for vehicle control cells compared to CN exposures. Values include three replicates performed in triplicate ($n = 9$).

where the effect value is represented as the mean response over all doses. For the sensitivity analyses, the effects of the exposure groups that included a cellulose material were compared to those of the untreated cells, where the effect value is represented as the slope of the dose-response relationship. Overall, the data indicated greater differences in the 4-hour exposure compared to the 15-minute exposures for all endpoints. SCNF and TCNF demonstrated a more significant influence than PCCNF at both time points, implying that these chemical compositions induce more substantial biological disruption. Most types influenced IL-6 mean, SCNF and PCCNF showed up earlier (some 15 min, some 4 h), while TCNF came in later (all 4 h). SCNF and TCNF affected GR, but again SCNF seemed to have a slightly earlier effect than TCNF. None of the types affected LDH. We conclude that the TEMPO functionalizing of CNF (*i.e.,* TEMPO-CNF (a method to oxidize cellulose using 2,2,6,6-tetramethylpiperidine-1-oxyl radical) induces a slightly delayed biological response.

These results are incorporated into the safer-by-design toolbox which was designed to be a screening tool for new functionalized CN, enabling side-by-side assessments or "read across" comparisons with conventional unmodified cellulose [39]. Ultimately, these efforts enable effective safety communication with regulatory agencies and industries. The data also prove valuable when addressing other safety concerns related to commercial applications, encompassing various exposure routes. These include inhaling dried cellulose during manufacturing or

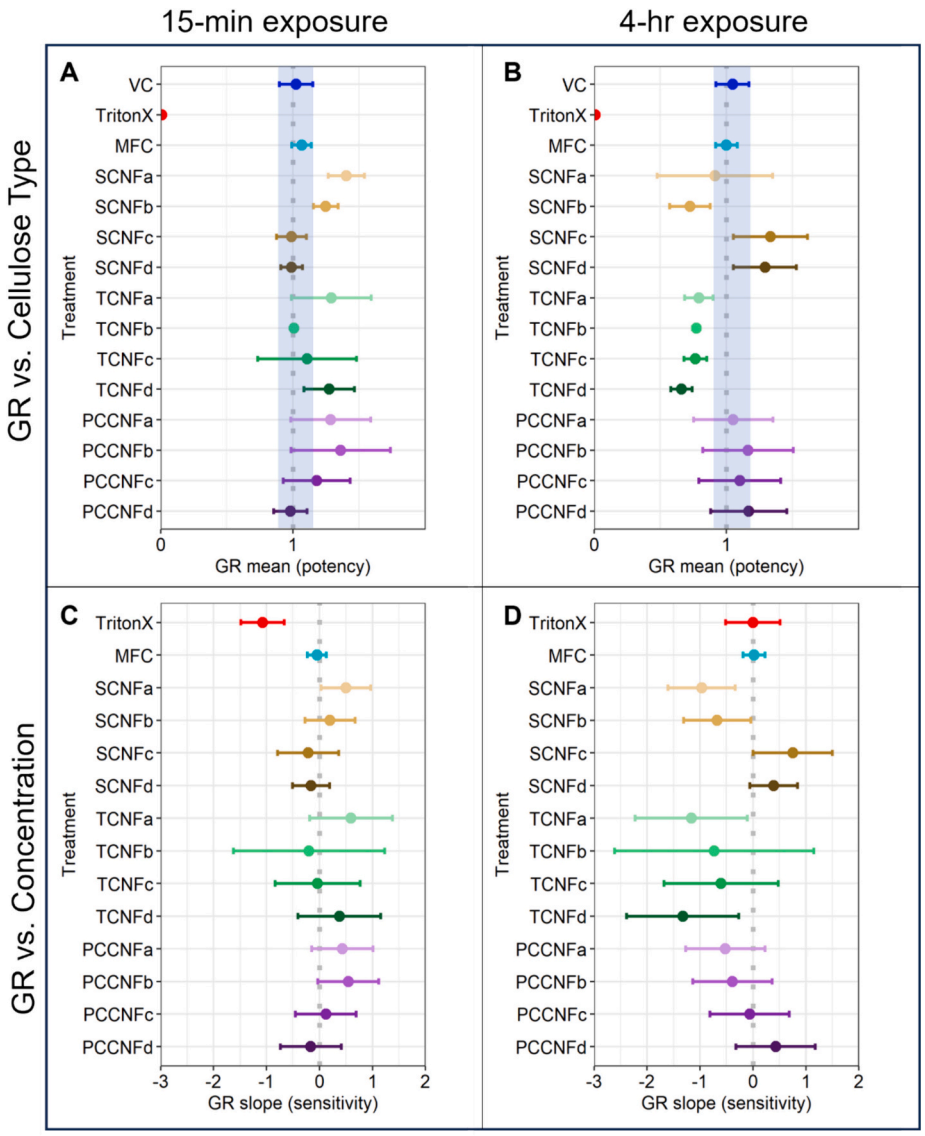

Fig. 10. Glutathione reductase slope *vs.* mean estimates of confidence. (A-B) GR *vs.* Cellulose Type. Estimated means with confidence intervals of GR expression *vs.* treatment, normalized to untreated cells. Intervals that contain 1 (intersecting the dotted line) are not significantly different (cannot reject the null hypothesis). The shaded blue bar indicates the VC comparison range. Sig (C—D) GR *vs.* Concentration. Estimated slopes with confidence intervals of GR expression *vs.* treatment concentration, normalized to untreated cells. Intervals that contain 0 (intersecting the dotted line) are not significantly different (cannot reject the null hypothesis).

Table 3
Statistically significant differences between each treatment *versus* untreated cells for mean (potency) and slope (sensitivity) across IL-6, GR, and LDH endpoints. Blue indicates a negative difference compared to untreated; red indicates a positive difference compared to untreated; gray indicates that the comparison is not applicable.

TREATMENT	15 min exposure						4 hr exposure					
	IL-6		*GR*		*LDH*		*IL-6*		*GR*		*LDH*	
	Potency	*Sensitivity*	*Potency*	*Sensitivity*	*Potency*	*Sensitivity*	*Potency*	*Sensitivity*	*Potency*	*Sensitivity*	*Potency*	*Sensitivity*
Pos. control												
MFC												
SCNFa												
SCNFb												
SCNFc												
SCNFd												
TCNFa												
TCNFb												
TCNFc												
TCNFd												
PCCNFa												
PCCNFb												
PCCNFc												
PCCNFd												

incorporation into building materials, potential dermal or ocular exposure through cosmetics, and the environmental impact of using modified celluloses in remediation processes. Exploring additional methods for assessing safety through these other exposure scenarios is necessary.

4. Conclusion

Our ongoing work examines the characteristics and effects of the most industrial-relevant and well-defined functionalization of cellulose *via* sulfation (chlorosulfonic acid hydrolyzed) and carboxylation (TEMPO-oxidized, periodate-chlorite oxidized) CNFs produced from high cellulose content dissolving pulp. We determined that the C6 carboxylated cellulose nanofibrils by TEMPO-oxidation induced the most toxicity in the biological model used in this study and that the observed effects were most prominent at the 4-hour post-exposure time points. These oral exposure safety findings using a three-dimensional gastrointestinal cell-based model provide a safety assessment and path forward for developing new cellulose materials.

The surface functionalities of CNs are critical to forming composite materials, laminates, barrier films, and coatings for food packaging applications. Several facile surface functionalized CNs have been demonstrated, and innovative CN production methods, such as maleic acid hydrolysis, have been developed to reduce the disadvantages of sulfuric acid hydrolyzed and TEMPO-oxidized CN production [61]. Despite promising new production methods and products, the impact on safety and toxicity in food packaging modifications has yet to be discovered. Therefore, our findings offer valuable data to researchers who aim to develop safer commercial cellulose products.

Supplementary data to this article can be found online at https://doi.org/10.1016/j.ijbiomac.2024.132603.

CRediT authorship contribution statement

Amanda K. Charlton-Sevcik: Writing – original draft, Methodology, Investigation, Formal analysis, Data curation. **Clancy Collom:** Methodology, Investigation, Formal analysis, Data curation. **You-Lo Hsieh:** Writing – review & editing, Resources, Formal analysis, Data curation, Conceptualization. **Nicole Stark:** Writing – review & editing, Funding acquisition, Conceptualization. **James D. Ede:** Software, Methodology, Investigation, Formal analysis, Data curation. **Jo Anne Shatkin:** Writing – review & editing, Project administration, Funding acquisition, Conceptualization. **Christie M. Sayes:** Writing – review & editing, Writing – original draft, Visualization, Supervision, Software, Resources, Project administration, Methodology, Investigation, Funding acquisition, Formal analysis, Data curation, Conceptualization.

Declaration of competing interest

The authors declare that they have no known competing financial interests or personal relationships that could have appeared to influence the work reported in this paper.

Data availability

Data will be made available on request.

Acknowledgements

The authors would like to thank the Department of Environmental Science and the funding partners of the Alliance for Food Safety Acceptance of Fibrillated and Crystalline Cellulloses (AFSAC) Consortium, including the P3Nano public-private partnership between the US Endowment for Forestry and Communities and the USDA Forest Service Forest Products Laboratory, for financially supporting this work. The authors also thank Dr. Alejandro Ramirez (BU) and the Mass Spectrometry Center for access to the ICP-MS.

Funding

The authors would like to thank the Department of Environmental Science and the funding partners of the AFSAC Public Private Partnership including the US Endowment for Forestry and Communities and the USDA Forest Service Forest Products Laboratory for financial support of this work.

References

[1] A.W. Carpenter, C.-F. de Lannoy, M.R. Wiesner, Cellulose nanomaterials in water treatment technologies, Environ. Sci. Technol. 49 (9) (2015) 5277–5287.
[2] A.H. Tayeb, E. Amini, S. Ghasemi, M. Tajvidi, Cellulose nanomaterials—binding properties and applications: a review, Molecules 23 (10) (2018) 2684.
[3] F. Li, E. Mascheroni, L. Piergiovanni, The potential of nanocellulose in the packaging field: a review, Packag. Technol. Sci. 28 (6) (2015) 475–508.
[4] M. Zhu, S. Huan, S. Liu, Z. Li, M. He, G. Yang, S. Liu, D.J. McClements, O.J. Rojas, L. Bai, Recent development in food emulsion stabilized by plant-based cellulose nanoparticles, Curr. Opin. Colloid Interface Sci. 56 (2021) 101512.
[5] A.B. Perumal, R.B. Nambiar, J. Moses, C. Anandharamakrishnan, Nanocellulose: recent trends and applications in the food industry, Food Hydrocoll. 107484 (2022).
[6] E. Lizundia, D. Puglia, T.-D. Nguyen, I. Armentano, Cellulose nanocrystal based multifunctional nanohybrids, Prog. Mater. Sci. 112 (2020) 100668.
[7] K. Nelson, T. Retsina, M. Iakovlev, A. van Heiningen, Y. Deng, J.A. Shatkin, A. Mulyadi, American Process: Production of Low Cost Nanocellulose for Renewable, Advanced Materials Applications, An industrial perspective of turning materials into new products, Materials research for manufacturing, 2016, pp. 267–302.
[8] J.K. Pandey, S. Ahn, C.S. Lee, A.K. Mohanty, M. Misra, Recent advances in the application of natural fiber based composites, Macromol. Mater. Eng. 295 (11) (2010) 975–989.
[9] T.C. Mokhena, M.J. John, Cellulose nanomaterials: new generation materials for solving global issues, Cellulose 27 (2020) 1149–1194.
[10] Y. Zhang, T. Nypelö, C. Salas, J. Arboleda, I.C. Hoeger, O.J. Rojas, Cellulose nanofibrils: from strong materials to bioactive surfaces, J. Renew. Mater. 1 (3) (2013) 195–211.
[11] A. Sharma, M. Thakur, M. Bhattacharya, T. Mandal, S. Goswami, Commercial application of cellulose nano-composites–a review, Biotechnol. Rep. 21 (2019) e00316.
[12] F. Jiang, Y.-L. Hsieh, Self-assembling of TEMPO oxidized cellulose nanofibrils as affected by protonation of surface carboxyls and drying methods, ACS Sustain. Chem. Eng. 4 (3) (2016) 1041–1049.
[13] D. Klemm, B. Heublein, H.P. Fink, A. Bohn, Cellulose: fascinating biopolymer and sustainable raw material, Angew. Chem. Int. Ed. 44 (22) (2005) 3358–3393.
[14] H.A. Khalil, Y. Davoudpour, C.K. Saurabh, M.S. Hossain, A. Adnan, R. Dungani, M. Paridah, M.Z.I. Sarker, M.N. Fazita, M. Syakir, A review on nanocellulosic fibres as new material for sustainable packaging: process and applications, Renew. Sust. Energ. Rev. 64 (2016) 823–836.
[15] H. Kargarzadeh, M. Mariano, D. Gopakumar, I. Ahmad, S. Thomas, A. Dufresne, J. Huang, N. Lin, Advances in cellulose nanomaterials, Cellulose 25 (2018) 2151–2189.
[16] J.D. Ede, K.J. Ong, M. Goergen, A. Rudie, C.A. Pomeroy-Carter, J.A. Shatkin, Risk analysis of cellulose nanomaterials by inhalation: current state of science, Nanomaterials 9 (3) (2019) 337.
[17] N. Vital, C. Ventura, M. Kranendonk, M. Silva, H. Louro, Toxicological Assessment of Cellulose Nanomaterials: Oral Exposure. Nanomaterials 2022, 12, 3375. In.: s Note: MDPI Stays Neutral With Regard to Jurisdictional Claims in Published, 2022.
[18] J.A. Shatkin, B. Kim, Cellulose nanomaterials: life cycle risk assessment, and environmental health and safety roadmap, Environ. Sci. Nano 2 (5) (2015) 477–499.
[19] A.F. Gualtieri, Towards a quantitative model to predict the toxicity/pathogenicity potential of mineral fibers, Toxicol. Appl. Pharmacol. 361 (2018) 89–98.
[20] D.B. Warheit, C.M. Sayes, K.L. Reed, K.A. Swain, Health effects related to nanoparticle exposures: environmental, health and safety considerations for assessing hazards and risks, Pharmacol. Ther. 120 (1) (2008) 35–42.
[21] A. Gajewicz, B. Rasulev, T.C. Dinadayalane, P. Urbaszek, T. Puzyn, D. Leszczynska, J. Leszczynski, Advancing risk assessment of engineered nanomaterials: application of computational approaches, Adv. Drug Deliv. Rev. 64 (15) (2012) 1663–1693.
[22] G. Oberdörster, A. Maynard, K. Donaldson, V. Castranova, J. Fitzpatrick, K. Ausman, J. Carter, B. Karn, W. Kreyling, D. Lai, Principles for characterizing the potential human health effects from exposure to nanomaterials: elements of a screening strategy, Part. Fibre Toxicol. 2 (1) (2005) 1–35.
[23] S. Halappanavar, J.D. Ede, I. Mahapatra, H.F. Krug, E.D. Kuempel, I. Lynch, R. J. Vandebriel, J.A. Shatkin, A methodology for developing key events to advance nanomaterial-relevant adverse outcome pathways to inform risk assessment, Nanotoxicology 15 (3) (2021) 289–310.
[24] J.A. Shatkin, Defining Risk Assessment and How It Is Used for Environmental Protection and Its Potential Role for Managing Nanotechnology Risks. In: Nanotechnology, CRC Press, 2017, pp. 31–60.
[25] H. Wang, P.C. Brown, E.C. Chow, L. Ewart, S.S. Ferguson, S. Fitzpatrick, B. S. Freedman, G.L. Guo, W. Hedrich, S. Heyward, 3D cell culture models: drug

pharmacokinetics, safety assessment, and regulatory consideration, Clin. Transl. Sci. 14 (5) (2021) 1659–1680.
[26] D. Zink, J.K.C. Chuah, J.Y. Ying, Assessing toxicity with human cell-based in vitro methods, Trends Mol. Med. 26 (6) (2020) 570–582.
[27] S. Adler, D. Basketter, S. Creton, O. Pelkonen, J. Van Benthem, V. Zuang, K. E. Andersen, A. Angers-Loustau, A. Aptula, A. Bal-Price, Alternative (non-animal) methods for cosmetics testing: current status and future prospects—2010, Arch. Toxicol. 85 (2011) 367–485.
[28] S.K. Balani, G.T. Miwa, L.-S. Gan, J.-T. Wu, F.W. Lee, Strategy of utilizing in vitro and in vivo ADME tools for lead optimization and drug candidate selection, Curr. Top. Med. Chem. 5 (11) (2005) 1033–1038.
[29] S.W. Baran, P.C. Brown, A.R. Baudy, S.C. Fitzpatrick, C. Frantz, A. Fullerton, J. Gan, R.N. Hardwick, K.M. Hillgren, A.K. Kopec, Perspectives on the evaluation and adoption of complex in vitro models in drug development: workshop with the FDA and the pharmaceutical industry (IQ MPS Affiliate), ALTEX-Alternat. Anim. Exp. 39 (2) (2022) 297–314.
[30] J.R. Sobus, J.F. Wambaugh, K.K. Isaacs, A.J. Williams, A.D. McEachran, A. M. Richard, C.M. Grulke, E.M. Ulrich, J.E. Rager, M.J. Strynar, Integrating tools for non-targeted analysis research and chemical safety evaluations at the US EPA, J. Expo. Sci. Environ. Epidemiol. 28 (5) (2018) 411–426.
[31] A.W. Knight, S. Little, K. Houck, D. Dix, R. Judson, A. Richard, N. McCarroll, G. Akerman, C. Yang, L. Birrell, Evaluation of high-throughput genotoxicity assays used in profiling the US EPA ToxCastTM chemicals, Regul. Toxicol. Pharmacol. 55 (2) (2009) 188–199.
[32] R.S. Thomas, T. Bahadori, T.J. Buckley, J. Cowden, C. Deisenroth, K.L. Dionisio, J. B. Frithsen, C.M. Grulke, M.R. Gwinn, J.A. Harrill, The next generation blueprint of computational toxicology at the US Environmental Protection Agency, Toxicol. Sci. 169 (2) (2019) 317–332.
[33] T.B. Knudsen, R.J. Kavlock, G.P. Daston, D. Stedman, M. Hixon, J.H. Kim, Developmental toxicity testing for safety assessment: new approaches and technologies, Birth Defects Res. B Dev. Reprod. Toxicol. 92 (5) (2011) 413–420.
[34] T. King, M. Cole, J.M. Farber, G. Eisenbrand, D. Zabaras, E.M. Fox, J.P. Hill, Food safety for food security: relationship between global megatrends and developments in food safety, Trends Food Sci. Technol. 68 (2017) 160–175.
[35] J.A. Shatkin, K.J. Ong, J.D. Ede, T.H. Wegner, M. Goergen, Toward cellulose nanomaterial commercialization: knowledge gap analysis for safety data sheets according to the globally harmonized system, TAPPI J. 15 (6) (2016) 425–437.
[36] J.A. Shatkin, K. Ong, J. Ede, Minimizing Risk: An Overview of Risk Assessment and Risk Management of Nanomaterials, Protocols and Industrial Innovations, Metrology and Standardization of Nanotechnology, 2017, pp. 381–408.
[37] K.J. Ong, J.D. Ede, C.A. Pomeroy-Carter, C.M. Sayes, M.R. Mulenos, J.A. Shatkin, A 90-day dietary study with fibrillated cellulose in Sprague-Dawley rats, Toxicol. Rep. 7 (2020) 174–182.
[38] J.D. Ede, K.J. Ong, M.R. Mulenos, S. Pradhan, M. Gibb, C.M. Sayes, J.A. Shatkin, Physical, chemical, and toxicological characterization of sulfated cellulose nanocrystals for food-related applications using in vivo and in vitro strategies, Toxicol. Res. 9 (6) (2020) 808–822.
[39] S.H. Pradhan, M.R. Mulenos, L.R. Steele, M. Gibb, J.D. Ede, K.J. Ong, J.A. Shatkin, C.M. Sayes, Physical, chemical, and toxicological characterization of fibrillated forms of cellulose using an in vitro gastrointestinal digestion and co-culture model, Toxicol. Res. 9 (3) (2020) 290–301.
[40] M.R. Mulenos, B. Zechmann, C.M. Sayes, Sample preparation utilizing sputter coating increases contrast of cellulose nanocrystals in the transmission electron microscope, Microscopy 68 (6) (2019) 471–474.
[41] T. Jiang, C.A. Amadei, N. Gou, Y. Lin, J. Lan, C.D. Vecitis, A.Z. Gu, Toxicity of single-walled carbon nanotubes (SWCNTs): effect of lengths, functional groups and electronic structures revealed by a quantitative toxicogenomics assay, Environ. Sci. Nano 7 (5) (2020) 1348–1364.
[42] F. Jiang, S. Han, Y.-L. Hsieh, Controlled defibrillation of rice straw cellulose and self-assembly of cellulose nanofibrils into highly crystalline fibrous materials, RSC Adv. 3 (30) (2013) 12366–12375.
[43] B. Pingrey, Y.-L. Hsieh, Sulfated cellulose Nanofibrils from Chlorosulfonic acid treatment and their wet spinning into high-strength fibers, Biomacromolecules 23 (3) (2022) 1269–1277.
[44] G. Patterson, Y.-L. Hsieh, Tunable dialdehyde/dicarboxylate nanocelluloses by stoichiometrically optimized sequential periodate–chlorite oxidation for tough and wet shape recoverable aerogels, Nanosc. Adv. 2 (12) (2020) 5623–5634.
[45] M. Minekus, M. Alminger, P. Alvito, S. Ballance, T. Bohn, C. Bourlieu, F. Carrière, R. Boutrou, M. Corredig, D. Dupont, A standardised static in vitro digestion method suitable for food–an international consensus, Food Funct. 5 (6) (2014) 1113–1124.
[46] M. Gibb, S.H. Pradhan, M.R. Mulenos, H. Lujan, J. Liu, J.D. Ede, J.A. Shatkin, C. M. Sayes, Characterization of a human in vitro intestinal model for the hazard assessment of nanomaterials used in cancer immunotherapy, Appl. Sci. 11 (5) (2021) 2113.
[47] G.M. DeLoid, Y. Wang, K. Kapronezai, L.R. Lorente, R. Zhang, G. Pyrgiotakis, N. V. Konduru, M. Ericsson, J.C. White, R. De La Torre-Roche, An integrated methodology for assessing the impact of food matrix and gastrointestinal effects on the biokinetics and cellular toxicity of ingested engineered nanomaterials, Part. Fibre Toxicol. 14 (2017) 1–17.
[48] C. Bisig, C. Voss, A. Petri-Fink, B. Rothen-Rutishauser, The crux of positive controls-pro-inflammatory responses in lung cell models, Toxicol. in Vitro 54 (2019) 189–193.
[49] C. Ventura, F. Pinto, A.F. Lourenço, P.J. Ferreira, H. Louro, M.J. Silva, On the toxicity of cellulose nanocrystals and nanofibrils in animal and cellular models, Cellulose 27 (2020) 5509–5544.
[50] R. Mu, X. Hong, Y. Ni, Y. Li, J. Pang, Q. Wang, J. Xiao, Y. Zheng, Recent trends and applications of cellulose nanocrystals in food industry, Trends Food Sci. Technol. 93 (2019) 136–144.
[51] Y. Zhuang, H. Peng, V. Mastej, W. Chen, MicroRNA regulation of endothelial junction proteins and clinical consequence, Mediat. Inflamm. 2016 (2016).
[52] W.-Y. Chen, M. Wang, J. Zhang, S.S. Barve, C.J. McClain, S. Joshi-Barve, Acrolein disrupts tight junction proteins and causes endoplasmic reticulum stress-mediated epithelial cell death leading to intestinal barrier dysfunction and permeability, Am. J. Pathol. 187 (12) (2017) 2686–2697.
[53] H. Yang, J.N. Rao, J.-Y. Wang, Posttranscriptional regulation of intestinal epithelial tight junction barrier by RNA-binding proteins and microRNAs, Tissue Barr. 2 (1) (2014) e28320.
[54] A. Moriyama, I. Ogura, K. Fujita, Potential issues specific to cytotoxicity tests of cellulose nanofibrils, J. Appl. Toxicol. 43 (1) (2023) 195–207.
[55] T. Heinze, Cellulose: structure and properties, in: Cellulose Chemistry and Properties: Fibers, Nanocelluloses and Advanced Materials, 2016, pp. 1–52.
[56] R. Kroes, C. Galli, I. Munro, B. Schilter, L.-A. Tran, R. Walker, G. Würtzen, Threshold of toxicological concern for chemical substances present in the diet: a practical tool for assessing the need for toxicity testing, Food Chem. Toxicol. 38 (2–3) (2000) 255–312.
[57] Y. Li, H. Jiao, H. Zhang, X. Wang, Y. Fu, Q. Wang, H. Liu, Y.-C. Yong, J. Guo, J. Liu, Biosafety consideration of nanocellulose in biomedical applications: a review, Int. J. Biol. Macromol. 130900 (2024).
[58] G. Singh, S. Saquib, A. Gupta, Environmental, legal, health, and safety issue of nanocellulose, in: Nanocellulose Materials, Elsevier, 2022, pp. 265–288.
[59] W. Brand, P.C. van Kesteren, E. Swart, A.G. Oomen, Overview of potential adverse health effects of oral exposure to nanocellulose, Nanotoxicology 16 (2) (2022) 217–246.
[60] N. Stoudmann, M. Schmutz, C. Hirsch, B. Nowack, C. Som, Human hazard potential of nanocellulose: quantitative insights from the literature, Nanotoxicology 14 (9) (2020) 1241–1257.
[61] Y.A.V. Villada, M.C. Iglesias, J. Zhu, N. Casis, M.S. Peresin, D.A. Estenoz, Carboxylated cellulose nanofibrils (R-CNFs) as an additive in water based drilling fluids (WBMs) applied to shale formations, Am. Chem. Soc. Sci. Meet. 1 (1) (2020).